Contents lists available at ScienceDirect

## Computer-Aided Design

journal homepage: www.elsevier.com/locate/cad



# Singularity Structure Simplification of Hexahedral Meshes via Weighted Ranking



Gang Xu<sup>a,b,\*</sup>, Ran Ling<sup>a</sup>, Yongjie Jessica Zhang<sup>c</sup>, Zhoufang Xiao<sup>a</sup>, Zhongping Ji<sup>a,b</sup>, Timon Rabczuk<sup>d</sup>

- <sup>a</sup> School of Computer Science and Technology, Hangzhou Dianzi University, Hangzhou 310018, China
- <sup>b</sup> Key Laboratory of Complex Systems Modeling and Simulation, Ministry of Education, Hangzhou 310018, China
- <sup>c</sup> Department of Mechanical Engineering, Carnegie Mellon University, USA
- d Institute of Structural Mechanics, Bauhaus-Universitat Weimar, Germany

#### ARTICLE INFO

Article history: Received 20 April 2019 Received in revised form 15 July 2020 Accepted 16 September 2020

Keywords:
Hex-mesh
Singularity structure simplification
Weighted ranking
Uniformity
Base complex

#### ABSTRACT

In this paper, we propose an improved singularity structure simplification method for hexahedral (hex) meshes using a weighted ranking approach. In previous work, the selection of to-be-collapsed base complex sheets/chords is only based on their thickness, which will introduce a few closed-loops and cause an early termination of simplification and a slow convergence rate. In this paper, a new weighted ranking function is proposed by combining the valence prediction function of local singularity structure, shape quality metric of elements and the width of base complex sheets/chords together. Adaptive refinement and local optimization are also introduced to improve the uniformity and aspect ratio of mesh elements. Compared to thickness ranking methods, our weighted ranking approach can yield a simpler singularity structure with fewer base-complex components, while achieving comparable Hausdorff distance ratio and better mesh quality. Comparisons on a hex-mesh dataset are performed to demonstrate the effectiveness of the proposed method.

© 2020 Elsevier Ltd. All rights reserved.

#### 1. Introduction

In recent years, the application of hexahedral (hex) meshes in finite element and isogeometric analysis has become increasingly widespread, because of its good numerical performance, small storage space requirements, and natural advantage of being able to construct tensor-product splines [1,2]. However, hex-mesh generation is not yet mature, and it cannot be guaranteed that a good quality initial mesh can be generated in all cases. For complex shapes and structural models, the octree-based mesh generation method was proposed [3-5]. This efficient method can ensure a topologically valid and well-formed meshing result. However, it generates a large number of cells and too many singularities. In some scenarios, we do not need a dense mesh and complicated interior structures. Meshes with simple structure and fewer singularities are more conducive to accelerating computational and convergence speed [6]. Therefore, it is very important to propose an effective singularity structure simplification method for hex-meshes.

Some research work has contributed to this topic in the past 10 years. In [7], an adaptive hex-mesh localization method was

E-mail address: gxu@hdu.edu.cn (G. Xu).

proposed. Topological operations such as collapsing and pillowing are used to process the locality, and localized roughening is maintained while maintaining topological connectivity and shape of the input mesh, which provides a basic idea of hex-mesh coarsening. In [8], the mesh structure is simplified according to the reparameterization requirements, and singularity is effectively reduced while maintaining the number of mesh elements. Template matching is used to split patches and eliminate the leading blocks. However, its implementation is very limited and not robust. It cannot simplify self-interleaved and closed-loops, resulting in poor results on input meshes obtained from octreebased methods. In [9], a robust hex-mesh structure simplification method was proposed. It is possible that a feasible solution with a simpler and coarser structure exists, but the algorithm might fail to find it. Especially, the ranking method for the selection of to-be-collapsed base complex sheets/chords is only based on the thickness, and it cannot guarantee to remove most of the singular structures. It will also introduce a few closed-loops and terminate the simplification process in advance. For an initial hex-mesh with many singular vertices, a proper priority ranking algorithm is needed to guide the simplification of the singularity structure. Moreover, a local parameterization is also needed to improve the mesh quality and repair topology structure after simplification.

<sup>\*</sup> Corresponding author at: School of Computer Science and Technology, Hangzhou Dianzi University, Hangzhou 310018, China.

In this paper, we propose an improved singularity structure simplification method of hex-meshes. The main contribution can be summarized as follows:

- A new weighted ranking approach for singularity structure simplification is proposed by combining the valence prediction function of local singularity structure, shape quality metric of elements and the width of base complex sheets/chords.
- A local optimization for SLIM [10] is proposed to improve the uniformity of hex-elements while maintaining the element quality;
- An adaptive sheet refinement method is proposed to improve the accuracy of boundary geometry approximation while maintaining similar number of hex-elements.

Based on these improvements, the proposed weighted ranking method can achieve a smaller number of singularities with comparable Hausdorff distance ratio, effectively remove the kinks in the hex-mesh.

The remainder of the paper is structured as follows. A review of related hex-mesh generation and mesh simplification is presented in Section 2. Some basic concepts and framework overview are described in Section 3. Section 4 presents the sheet and chord collapsing operation of base-complex. The proposed weighted ranking approach is described in Section 5. Adaptive sheet refinement is presented in Section 6. In Section 7, the experimental results are illustrated. Finally, the paper is concluded and future work is outlined in Section 8.

#### 2. Related work

In this section, some related work on hex-mesh generation and simplification will be presented.

Hexahedral mesh generation. Hex mesh has been widely studied for decades. However, an automatic method that can generate high quality hex-meshes for any complex geometry is still unavailable because of the strong topological constraints [11], i.e., the dual chord and the dual sheet. Some methods were devised for specific types of geometries. For example, the mapping method is preferable for mappable geometries, while the sweeping method [12] is often used for swept volumes. By combining with domain partition, they can be applied to complex geometries [12-14]. Based on the idea of paving, several geometric and topological approaches have been proposed for all-hex meshing. Plastering [15] and H-Morph [16] generate layers of hex elements in geometric ways, whereas the whisker weaving [17,18] method uses spatial twist continuum and generates the topological dual of hex-mesh. Unconstrained plastering [19] is extended from plastering. Different from other paving methods, it starts from propagating the original geometry boundary instead of a pre-meshed boundary into the interior domain, and hex elements are generated when three propagating fronts intersect each other. The octree-based approach [20] is very robust and can be executed in a highly automatic way, however, it yields poor quality elements near boundary and the final mesh heavily relies on the orientation of the coordinate system. The polycube based meshing approach uses a low distortion mapping between the input model and polycube, and computes the corresponding volumetric mappings. The deformation methods are introduced for polycube construction [21–25], and frame fields are proposed to guide the polycube construction [26]. In [27], Nieser et al. compute a global parameterization of the volume on the basis of a frame field to construct hex-meshes. Theoretical conditions on singularities and the gradient frame field are derived for degenerated parameterization, and badly placed singularities can lead to distortion. Based on spherical harmonics representation, Huang et al. [28] generated a boundary-aligned smooth frame field by minimizing an energy function, and Li et al. also proposed the singularity-restricted field [29]. Though impressive results were obtained from the frame field based approaches, further efforts are still needed for practical use.

Mesh simplification. Mesh simplification generally reduces the number of elements and maximizes the appearance of the original mesh by performing local coarsening operations. Triangular elements can be combined with the edge flipping operation and local MLS (moving least-squares) form of the minimum energy function [30]. This method was also applied to hierarchical mesh generation with iterative simplification. In quadrilateral and hex-mesh simplification, similar local operations were also proposed [31,32]. Sheets and chords are extracted by the inherent dual structure, and the local operation is simplified for the object [8,9]. Recent progress in structure simplification has achieved great success in polycube simplification [33] and hex-mesh optimization [34]. In [35], an effective approach was proposed to simplify the surface meshes of arbitrary polygonal type to quadonly meshes based on the key-frame mapping on base domains, and in [33], the singularity misalignment problem was solved directly in the polycube space, and the corner optimization strategy was introduced to produce coarser block structured surface and volumetric meshes. Moreover, the induced meshes are suited for spline fitting. Topology control operations in hex-mesh simplification can also be applied to adjusting low quality mesh elements. In [34], an adjustment strategy for repairing the inverted elements was proposed by combining the basic mesh editing operations with frame field optimization. Based on the singularity structure in the mesh, a base-complex block structure is extracted in [9]. Then the simplification operation is performed to collapse base complex sheets and chords while redistributing the distortion based on a volumetric parameterization.

## 3. Basic concepts and framework overview

In this section, we will introduce some basic concepts on hex-mesh and the overview of the proposed framework.

## 3.1. Base-complex

The proposed hex-mesh simplification can effectively reduce the singularity structure while maintaining the specified number of elements. We briefly introduce the definition of singularity structure, base-complex and two types of structure called basecomplex sheet and base-complex chord. The valence of vertex, edge and face is denoted as the number of its neighboring hex elements. A vertex is said to be regular if its valence is 4 on the boundary or 8 in the interior. Similar to the regular vertex, an edge is regular when its valence is 2 on the boundary or 4 in the interior. Then a series of connected irregular edges with the same valence compose of a singular edge, and its two ending vertices are called singular vertices, except the case of closed singular edges. The singularity structure is composed of these singular edges and singular vertices. According to the above definitions, we can extract the singularity structure of a hexmesh. Each singular edge with a valence of n can be extended to n segmented surfaces, and the valid manifold hex-mesh can be divided into cube-like components by these segmented surfaces (refer to [8] for more details). A segmented structure called basecomplex can be extracted in this way. The base-complex of the hex-mesh M is denoted as  $B = (B_V, B_E, B_F, B_C)$ , where  $B_C$  is the set of cube-like components (composed of hex elements),  $B_V$  and  $B_E$  are the set of 8 corners of each cube-like component and the set of base-complex edges (a series of connected edges between two base-complex vertices) respectively, and  $B_F$  contains base-complex faces of each component.

**Fig. 1.** (a) The base-complex sheet (green elements with mesh lines) consists of the left surface  $F_L$ , the right surface  $F_R$  and the middle volume  $E_M$ , with the edge pair (yellow edges) and the vertex pair (red dots) shown in (b). (c) The green elements form a base-complex chord, where  $F_L$  and  $F_R$  in (d) can be determined from the main diagonal direction. (For interpretation of the references to color in this figure legend, the reader is referred to the web version of this article.)

## **Algorithm 1** Framework of singularity structure simplification

**Input:** A hex-mesh M; target number of mesh elements,  $N_c$ ; target simplification ratio of components R; user-specified threshold of Hausdorff distance ratio, HR;

**Output:** Hex mesh with a simplified base-complex,  $M_{out}$ ;

- 1: Extract the base-complex structure  $B = (B_V, B_E, B_F, B_C)$  from M.
- 2: Extract all the base-complex sheets and chords satisfying filtering criteria, then push them into two priority queues  $S_{sheet}$  and  $S_{chord}$  with length  $k_s$  and  $k_c$  respectively based on the proposed weighted ranking approach. When the number of mesh elements is less than  $N_c$ , go to Step 5;
- 3: Find the top-ranked base-complex sheet and  $min(\lfloor k_c/k_s \rfloor, 3)$  base-complex chords to perform removing operation in *Step 4*, the order of removing follows the sequence in  $S_{sheet}$  and  $S_{chord}$ ;
- 4: Remove the sheet/chord by collapsing operation, then perform reparameterization with local regularization smoothing. If a valid mapping parameterization is not found or the quality metric is below the threshold, remove the next sheet/chord until a successful operation is performed (If the candidates selected in *Step 3* are all invalid, the next candidate will be found in *S*<sub>sheet</sub> and *S*<sub>chord</sub> in order). If any candidates in *S*<sub>sheet</sub> and *S*<sub>chord</sub> can not be successfully removed, go to *Step 5* directly;
- 5: If the number of elements is smaller than  $N_c$  or the Hausdorff distance ratio is larger than HR, perform adaptive refinement; if the specified simplification ratio R is not satisfied, go back to  $Step\ 1$ ;
- 6: After finishing the simplification process, perform a global optimization operation, return  $M_{out}$ .

Base-complex sheet and base-complex chord can be extracted based on the base-complex structure. Since the singularities are located at its eight corners and three groups of four topologically parallel base-complex edges, removing components can effectively simplify singularity structure by collapsing base-complex sheets and chords. The base-complex sheet S consists of three parts: the left surface  $F_L$  (or the right surface  $F_R$ ) contains all base-complex vertices, edges and faces in the boundary of the left (or right) part, and the middle volume  $E_M$  contains the base-complex edges with two end nodes on  $F_L$  and  $F_R$  respectively. Topology elements in  $F_L$  and  $F_R$  can form element groups. Base-complex chord has a similar definition, in which two sides follow the main diagonal direction. Fig. 1 shows the structure of base-complex sheet and base-complex chord.

#### 3.2. Framework overview

In this paper, we propose an improved singularity structure simplification method for hex-meshes while maintaining the shape boundary and the target number of element. The proposed framework consists of the following steps as shown in Algorithm 1:

Step 1. Specification of simplification parameters. In this step, we will specify the target number of mesh elements  $N_c$ , target simplification ratio of components R and threshold of Hausdorff distance ratio HR for an input hex-mesh M, in which R is denoted as

$$R = 1 - \frac{\#BC_{final}}{\#BC_{init}}$$

in which  $\#BC_{init}$  and  $\#BC_{final}$  are the number of base-complex components in the input hex-mesh and the output hex-mesh respectively;

- Step 2. Extraction of base-complex sheets/chords based on the singularity structure of the input hex-mesh as described in Section 3.1.
- Step 3. Weighted ranking of base-complex sheets/chords by combining the valence prediction function of local singularity structure, shape quality metric of elements and the width of base complex sheets/chords.
- Step 4. Find the top-ranked base-complex sheets and base-complex chords iteratively and perform collapsing operation with reparameterization. This pipeline will be terminated if the output hex-mesh satisfies the target simplification ratio.
- Step 5. Adaptive sheet refinement is performed to obtain a similar number of hex-elements as the target number of hex-elements. This step can improve the hex-element uniformity and reduce the error between the input and output hex-mesh geometry. To locally improve the uniformity and aspect ratio, we also propose a local regularization optimization in the parameterization for sheet/chord collapsing.

With the proposed method, the singularity structure complexity of a hex-mesh decreases rapidly. Furthermore, a few close-loops and entangled sheets can be commendably eliminated, leading to a high simplification rate. In addition, two extra ranking terms are adopted to maintain the element quality and shape boundary. In the following sections, a detailed introduction will be given for each step.

#### 4. Coarsening operators on hex-meshes

In this section, we introduce two local coarsening operations on hex-meshes: the base-complex sheet collapsing operation and the base-complex chord collapsing operation, which are two generalized concepts to reduce singularity structure complexity of hex-meshes. The base-complex sheet collapsing operation is mainly applied to change singularities globally, while the base-complex chord collapsing operation is used locally, especially for removing edge pairs with a valence of  $3\sim5$ . These two operations may introduce non-manifold and doublet configurations as

shown in Fig. 2. Moreover, the collapsing operations may lead to local higher complexity which should be prevented. Hence, several filtering criteria will be proposed to determine whether there are problematic cases.

#### 4.1. Base-complex sheet collapsing operation

A base-complex sheet collapsing operation similar to [9] will be adopted here. Both sides of a sheet can be found by components, and then we remove the middle part of the base-complex sheet and preserve the side of  $F_L$  or  $F_R$ . Finally, parameterization is employed to relocate these vertices within the  $\delta$ -ring neighborhood region ( $\delta$  is set to be 4 as in [9]). Before sheet collapsing, several filtering criteria are used to detect whether it should be put into the priority queue. The vertex relocation problem after a collapsing operation can be solved by an energy-minimizing parameterization method [9]. The corresponding energy function can be defined as follows:

$$\min_{V} E(V) = E_D(V) + \lambda_t E_T(V) + \lambda_b E_B(V),$$

in which V is the set of vertices,  $\lambda_t$  and  $\lambda_b$  are penalty coefficients,  $E_D(V)$  is the geometric distortion measurement of hexahedra,  $E_T(V)$  encourages two sides of a sheet to collapse into its dual sheet,  $E_B(V)$  is related to the deviation between the original position and new position of vertices on boundary [9]. The definition of  $E_D(V)$ ,  $E_T(V)$  and  $E_B(V)$  can be referred to Appendix. 1 for details.

**Valence prediction.** When edge pairs in  $F_L$  and  $F_R$  are collapsed into a single edge, then the corresponding edge valence may be changed. Generally, the valence of an inner edge is greater than 2, otherwise, the adjacent elements will be degenerated or form a doublet configuration (two hexahedra share two or more faces as shown in Fig. 2), which is forbidden in our framework, and the valence of the created edge on surface is less than the valences of edge pair is also forbidden, which will break the topology continuity. For the edge pair of  $e_l$  and  $e_r$  in a non-self-intersection sheet, if the new edge is denoted as  $e_n$ , then the valence of  $e_n$  can be computed as follows:

$$v(e_n) = \begin{cases} v(e_l) + v(e_r) - 2, & f_{lr} \text{ is on boundary} \\ v(e_l) + v(e_r) - 4, & f_{lr} \text{ is not on boundary} \end{cases}$$
(1)

where v(e) is the valence of a base-complex edge, and the base-complex face  $f_{lr}$  directly connects  $e_l$  and  $e_r$ .

**Boundary shape**. The feature vertices/lines are extracted in the initialization stage as same as [9] (they are extracted by dihedral angle thresholding method), and in order to preserve sharp features, the sheet and chord containing sharp feature vertices are not allowed to be removed. Moreover, the base-complex sheet is not collapsed when the feature edges lie on base-complex edges. In the collapsing operation, we use a similar way for hex-mesh sheet collapsing. In the optimization step, local parameterization [9] is adopted. The boundary shape error and interior distortion will be distributed to  $\delta$ -ring neighboring elements by solving the energy minimization of geometric distortion and the quality of elements with the approach called scalable locally injective mapping (it is referred to as SLIM in the paper) in [10].

#### 4.2. Base-complex chord collapsing operation

The base-complex chord collapsing operation is mainly used to optimize bad singularity structure locally. It only has effect on one column of base-complex components. Different from chord collapsing in hex-mesh that merging four vertices per group into a new position, Fig. 2 shows the 3D case of chord collapsing. We extract two pairs of opposite base-complex edges, and

merge them along the diagonal direction, the relocation method of vertices after collapsing is same as base-complex sheet. The collapsing direction is denoted as the main diagonal direction and the orthogonal direction along boundary is referred as the sub-diagonal direction.

**Collapsing direction.** The collapsing direction can be chosen in two directions, the valences of base-complex edges in two sides along the main diagonal direction may change. Here, we only consider the four groups of topology-parallel base-complex edges on the chord surface following the direction of dual string. We compute the predicting valence of these created base-complex edges, and obtain the valence difference between the created edge and the regular edge. We aim to remove edge pairs with a valence of  $3\sim5$  and introduce high valence singularities as less as possible. In this paper, we measure the difference between the predicted valence and the regular valence by the following term

$$D_{v}(c) = \sum_{i=1}^{k} (\left| (v(e_{p1}^{i}) - 1) - p(e_{p1}^{i}) \right| + \left| (v(e_{p2}^{i}) - 1) - p(e_{p2}^{i}) \right| + \left| (v(e_{l}^{i}) + v(e_{r}^{i}) - 2) - \min(p(e_{l}^{i}), p(e_{r}^{i})) \right|),$$

$$D(c) = \min(D_{v1}(c), D_{v2}(c)), \qquad p(e) = \begin{cases} 2, & e \in E_{surface} \\ 4, & e \in E_{inner} \end{cases}$$

where  $e_{p1}^i$  and  $e_{p2}^i$  are the ith base-complex edges in the subdiagonal direction,  $e_l^i$  and  $e_r^i$  are the ith base-complex edges in the main diagonal direction as shown in Fig. 2, k is the number of contained components of the base-complex chord c,  $E_{surface}$  and  $E_{inner}$  are the ith set of boundary edges and inner edges respectively. We choose the optimal collapsing direction by minimizing D(c), the predicted valence of two optional directions are  $D_{v1}(c)$  and  $D_{v2}(c)$  respectively. In our experiments, we implement an easy-to-detect method in advance to improve efficiency, the chord collapsing operation is not allowed when D(c)/3k > 0.9, or the four groups of parallel edges following the direction of dual string contain more than two singular edges. This kind of chord will not be pushed to the priority queues.

Base-complex sheet collapsing can make significant impact on mesh globally, but it is extremely difficult to remove self-intersection sheets with complex tangles and close-loop configurations without creating vertices with high valence. Base-complex chord collapsing is used to eliminate the entangled regions, and it contributes to improving the simplification ratio of sheets.

## 4.3. Local parameterization for uniformity improvement

After collapsing arbitrary sheets/chords, we use local parametrization based on SLIM framework [9,10] to relocate vertices within the collapsing region, and reduce the distortion by adjusting the ideal shape for each hexahedron to satisfy the requirement of high uniformity. The framework of SLIM uses the local/global algorithm [36], and solves the distortion term globally while fixing the rotation as computed in the local step. In 3D case, the mapping from the original tetrahedral element to a deformed shape in a local orthogonal frame can be denoted as a Jacobian, and the deformation can be expressed indirectly by a transformation from the tetrahedron with three orthogonal edges to both shapes as shown in Fig. 3. The mapping between the reference element  $t_R$  to the original element  $t_I$  is defined as  $W_I$ . Similarly, the mapping between the reference element  $t_R$  and the deformed element  $t_D$  is defined as  $W_D$ . Since  $W_D$  and  $W_I$  are constant matrices for affine transformation, finally the Jacobian  $\phi$ of  $t_I \rightarrow t_D$  can be denoted as

$$\phi = W^D \circ (W^I)^{-1}. \tag{3}$$

Our experiments show that adjusting the Jacobian of a transformation to the target shape in a local operation can lead to

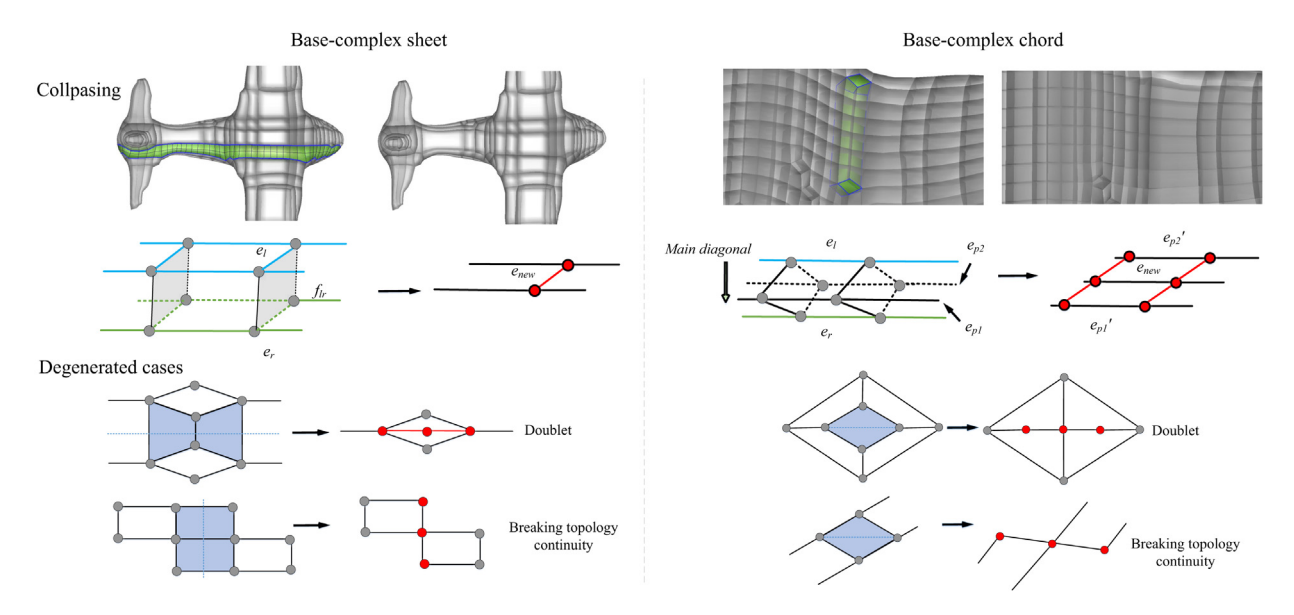


**Fig. 2.** Left: Base-complex sheet collapsing operation and 2D degenerated cases; Right: Base-complex chord collapsing operation and 2D degenerated cases. The blue base-complex edge  $e_l$  is contained in  $F_L$ , the green base-complex edge  $e_r$  is contained in  $F_R$ , the gray face linking a pair of  $e_l$  and  $e_r$  is  $f_{lr}$ , and the red components may change the edge valence. (For interpretation of the references to color in this figure legend, the reader is referred to the web version of this article.)

an ideal mesh result after global simplification. In this paper, we also propose a local optimization strategy to move vertices within the collapsing region during parameterization. For edges in the collapsing region, their length will be re-scaled while maintaining the element quality. A simple Laplace smoothing is performed as a local operation. Since SLIM is used frequently in collapsing and local refinement, and the number of elements in parameterized region has large variations, for the purpose of improving efficiency of SLIM, the iterative form is adapted instead of solving a large linear system.

Let M = (V, K) be the mesh of the parameterized region, V is the set of nodes, and K is the topology connectivity between vertices in the parameterized region, including nodes  $\{i\}$  and edges  $\{i,j\}$ . The discrete operator on M is defined as

$$(Lv)_i = \sum_i \omega_{ij}(v_i - v_j), \tag{4}$$

in which  $\omega_{ij}$  are the weights, and the iterative form can be defined

$$v_i^k = \sum_{j=1}^{N_i} w_{ij} v_j^{k-1} / N_i, \quad (\omega_{ij} = 1, \quad v_i, v_j \in V_{in}, \quad k = 1, 2, 3...)$$

and the iteration is terminated when the threshold of variance  $\epsilon$  is reached

$$\frac{\left[\sum_{i}(v_{i}^{k}-v_{i}^{k-1})^{2}\right]^{1/2}}{\left[\sum_{i}(v_{i}^{k-1}-v_{i}^{k-2})^{2}\right]^{1/2}} < \epsilon, \quad (k > 2)$$
(6)

where i and j are the vertex labels, k is the number of iterations,  $N_i$  is the number of neighboring vertices of the jth vertex,  $V_{in}$  is the set of inner vertices in parameterized region. Uniform weighting in the smoothing operation often introduces elements with low quality. In order to improve the orthogonality, the weighting scheme proposed in [37] is used to optimize the mesh locally. After volumetric smoothing, the regularized length of edges in each element is computed. A similar regularization process described in [9] is adapted, then we perform local parameterization with SLIM which uses the regularized results as the ideal mapping shape for each element.

#### 5. Weighted ranking for structure simplification

Many hex-mesh generation approaches such as octree-based and polycube methods often yield unnecessary singularities with a large number of small components in base-complex. The number of singularities can be progressively decreased by performing collapsing operations based on components, and the simplified singularity structure is obviously different with various collapsing sequences. After comparison with experimental data, we find that the collapsing order of base-complex sheets and chords has a significant effect on the final simplification results. In this paper, a weighted ranking sequence is introduced, which can choose the optimal candidate to be removed iteratively. The ranking sequence aims to remove singularities within fewer iterative steps. We formulate this problem as an energy minimization framework, and introduce a valence term related to the valence difference caused by collapsing to achieve a rapid removal of singularities. On the other hand, some constraints are included, for example, the resulting elements should not be inverted and the max Hausdorff distance ratio HR should be kept. Therefore, the sheet/chord removal leading to less mesh distortion will have the collapsing priority. From this motivation, we also introduce two extra ranking terms, called the distortion term and the width

## 5.1. Ranking method of base-complex sheet

In the base-complex sheet ranking sequence, we combine the valence term  $E_{sv}$ , the distortion term  $E_{sq}$  and the width term  $E_{sd}$  as the normalized form [38]. The ranking function which can greatly improve the simplification rate of base-complex components is defined as

$$E_s(s) = k_{sq}(1 - e^{-E_{sq}(s)}) + k_{sd}(1 - e^{-E_{sd}(s)}) + k_{sv}(1 - e^{-E_{sv}(s)})$$
 (7)

in which  $k_{sv}$ ,  $k_{sd}$  and  $k_{sd}$  are weights of different ranking terms. In our implementation, the width term  $E_{sd}(s)$  has the biggest weight, i.e.,  $k_{sv} = 0.4$ ,  $k_{sd} = 0.6$  and  $k_{sq} = 0.2$ . We also restrict the value of each term within (0, 2) to reduce the impact of the actual numerical size. In Fig. 4, we provide a comparison example of the first collapsing operation for different ranking terms  $E_{sq}$ ,  $E_{sd}$ ,  $E_{sv}$ ,  $E_{s}$  and the thickness term  $E_{thickness}$ .

(5)

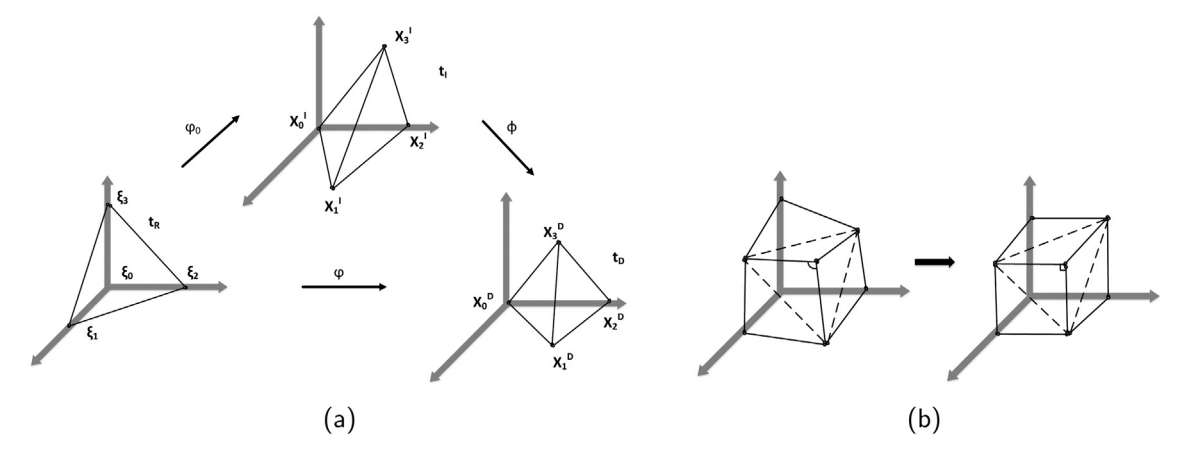


Fig. 3. (a) The mapping from a reference tetrahedron (left) to the origin shape (middle) and deformed shape (right). (b) The mapping of five tetrahedra in a hex element (left) to the element with ideal shape (right).

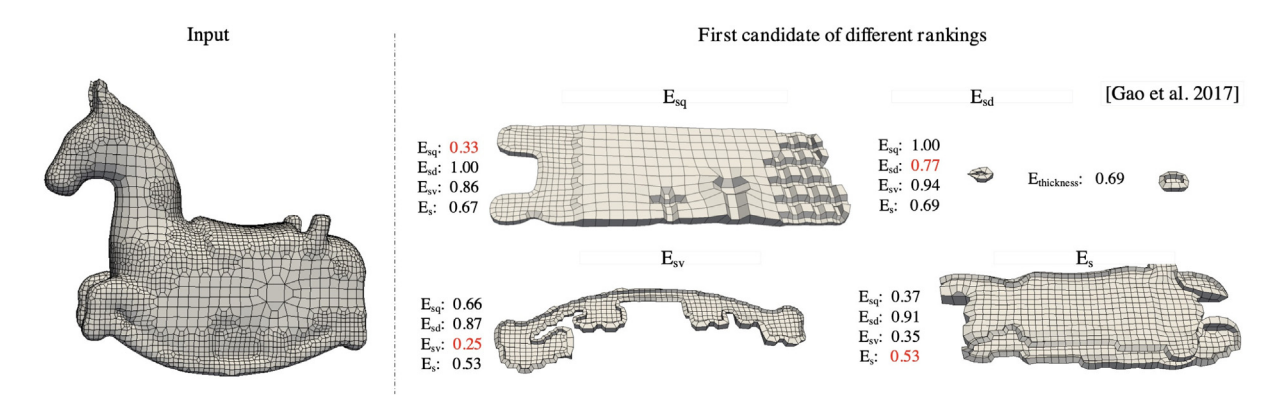


Fig. 4. A comparison example of the first candidate for different ranking term  $E_{sq}$ ,  $E_{sd}$ ,  $E_{sv}$ ,  $E_{s}$  and the thickness term  $E_{thickness}$ . The values of different ranking term are also provided.

**Valence term**. The proposed weighted ranking algorithm for base-complex sheet collapsing mainly focuses on the valence difference of singular edges during the simplification. As shown in [9], the singularities of a hex-mesh can be progressively simplified within a finite number of iterations. In this paper, we propose an indirect energy function of valence difference between the current mesh and the mesh without singularities. For the mesh with singular base-complex edges set  $S = \{e \mid e \in B_E \mid e \text{ is singular}\}$ , the energy function is defined as

$$E(M) = \sum_{e \in S} |v(e) - p(e)|.$$
 (8)

Since the simplification process is based on two kinds of collapsing operations, and the singular edges are only located in  $F_L$ ,  $F_R$  and  $E_M$ , then the energy function E(M) has a local representation on the base-complex sheet when it is collapsed

$$E(M) = \sum_{i=0}^{n} \left( -\sum_{e_M \in E_M^i} |v(e_M) - p(e_M)| + 1/v(e_{lr}) \sum_{e_{lr} \in F_L^i, F_R^i} |v(e'_{lr}) - p(e_{lr})| \right)$$
(9)

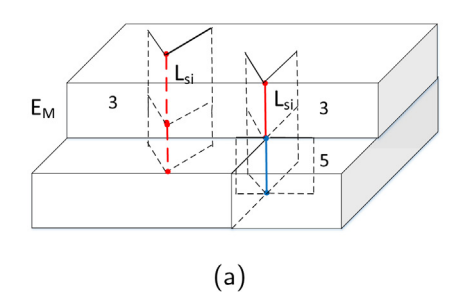
where i is the index of the base-complex sheet to be collapsed,  $E_M^i$  is the interior part of ith base-complex sheet,  $F_L^i$  and  $F_R^i$  are the left surface and the right surface of the ith base-complex sheet,  $e_M$  is the base-complex edge in  $E_M^i$  of the base-complex sheet,  $e_{lr}$  is the base-complex edge to be collapsed,  $e_{lr}'$  is the created new base-complex edge, and n is the number of the base-complex sheets

which are allowed to be collapsed. In order to prevent double-counting of difference (if the valence of the interior singular edge is k, k > 2, this singular edge is shared with k sheets), the value of coefficient is selected as the reciprocal of valence.

According to the energy function E(M), some analysis on the structure of base-complex sheets can be performed. The base-complex sheet has an interesting property: all the interior edges which are topology parallel to the dual face of sheet are regular, the singular edges only exist in  $E_M$  or  $F_L$  and  $F_R$ , and the collapsing operation will introduce edges with a different valence. Hence, the influence of collapsing operation can be predicted.

During a collapsing operation, the edges in the interior part will be eliminated. For a singular edge  $L_{si}$ , if the whole edge is contained in  $E_M$ , then the value of E(M) will be reduced. This type of elimination is equivalent to creating new regular edges while collapsing. Moreover, the singularity structure will not change when the singular edge  $L_{si}$  runs though the sheet ( $L_{si}$  is part of a singular edge). Such base-complex edges will not be considered in our valence calculation. Two types of  $L_{si}$  are shown in Fig. 5(a).

Since a singular edge is completely contained in  $F_L$  or  $F_R$  of one or more base-complex sheets, the collapsing operation may remove the singular edges in both sides directly. Concerning the valence variation of edges in an edge pair of  $F_L$  and  $F_R$ , the following three cases are shown in Fig. 5(b) respectively will be considered: (c1) all the edges in  $F_L$  and  $F_R$  are regular; (c2) edges in only one side of  $F_L$  or  $F_R$  are singular; and (c3) both edges in  $F_L$  and  $F_R$  are singular. In case of (c1), the valence of the created edge will be regular; in case of (c2), the created edge will have the same valence as an irregular edge, and it does not affect the surrounding singularity configurations; in case of



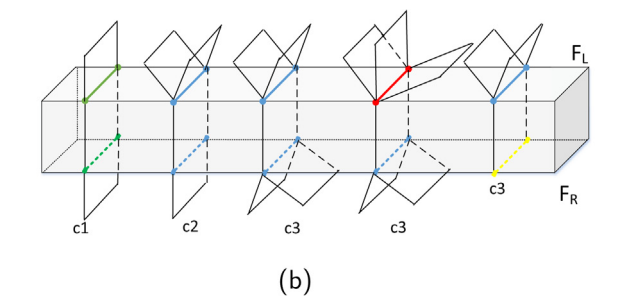


**Fig. 5.** Distribution of singularities in  $E_M$ ,  $F_L$  and  $F_R$ . The lines marked in green and black are regular edges, and all the other edges are singular edges. Two types of middle edges in  $E_M$  are shown in (a), and three types of edge pairs on both sides are shown in (b). (For interpretation of the references to color in this figure legend, the reader is referred to the web version of this article.)

(c3), the valence of created edges will change, which means that the singularities of the rest part of hex-mesh will be changed. Moreover, there are several configurations in case of (c3), the created edges might have different valences compared with base-complex edge pairs in  $F_L$  and  $F_R$ . The singularity structure will be simplified when the valence difference between irregular and regular edges decreases.

In order to improve the convergence rate of E(M), we greedily select the base-complex sheets which can effectively reduce E(M) locally and introduce edges with higher valence as few as possible. The valence term is defined as

$$E_{sv} = [DM - \beta(\sum_{i} T(K_i^{max} - K_i^{new}) + \sum_{i} K_i^{m})]/DM,$$
(10)

in which

$$\begin{cases} K_{i}^{new} = \left| v(e_{i}^{new}) - p(e_{i}^{new}) \right|, \\ K_{i}^{m} = \left| v(e_{i}^{m}) - p(e_{i}^{m}) \right|, \\ K_{i}^{max} = \max \left( \left| v(e_{i}^{l}) - q(e_{i}^{l}) \right|, \left| v(e_{i}^{r}) - q(e_{i}^{r}) \right| \right), \\ T(k) = \begin{cases} 0.5k, & k < 0 \\ 1.0, & k = 0 \\ k, & k > 0 \end{cases} \end{cases}$$

where i is the index of edge pairs,  $e_i^l$  and  $e_i^r$  form an edge pair, and they belong to  $F_L$  and  $F_R$  respectively,  $e_i^m$  is the singular edge in  $E_M$ , DM is a large value to control the scale of the term  $E_{Sv}$ , which is set as the maximum number of  $E_M$  in the hex-mesh. In our experiments,  $\beta$  is set to be 1.67. In order to minimize the energy function, the convergence rate will be faster when the value of  $\beta(\sum_{i=0}^n T(K_i^{max} - K_i^{new}) + \sum_i K_i^m)$  is much larger. Here T(k) is used to adjust the difference of valence, the speed of simplification will be slower and the simplification rate will be reduced while strict restriction is applied, hence the coefficient is set to be 0.5k when k < 0. For the difference as k = 0, it corresponds to the case that merging an inner singular edge and a boundary singular edge with the same valence, this kind of merging actually removes a singular edge, and the value of T(k) for k = 0 can be maintained less than the value for k > 0, hence we set the corresponding coefficient as 1.

**Distortion term.** The distortion term  $E_{sq}$  is an optional term for hex-mesh with complex singularity structure. The sheet passing through the regions with dense singularities often contains patches with serious distortion, hence removing these sheets can greatly improve the average value of Jacobians, and lead to a significant complexity reduction in geometric processing. Here we use the shape metric  $f_{shape}$  of hexahedron [39] to measure the sheet distortion.  $f_{shape} = 1$  if the hexahedron is a cube with parallel faces, and  $f_{shape} = 0$  if the hexahedron is degenerated.  $f_{shape}$  is a scale-invariant, the specific form adapted is given in Appendix A (refer to [39] for the specific definition of  $f_{shape}$ ).

In this paper, we obtain the second derivative of  $f_{shape}$  in each element for three parametric directions, and select the maximum difference as the differential value of the hexahedron. From the experiments, we find that serious distortion happens when the second derivative is up to 0.55 as illustrated in Fig. 6. In this term, we use the second derivative of  $f_{shape}$  to identify the regions with big distortion. Since local parameterization can improve the element quality, removing regions with serious distortion in advance will increase the average value of Jacobians locally. The value of  $\sum_{i=1}^n f_i$  has a large variation in different base-complex sheets, in order to obtain a reasonably weighted sum with the other terms, the distortion term needs to be normalized.  $\ln(x+e)^{-1}$  is used to restrict the value in [0,1).  $E_{sq}$  is defined as

$$E_{sq}(s) = \ln(\sum_{i=1}^{n} f_i + e)^{-1},$$
(11)

$$f_i = \begin{cases} 0, & d(i) < 0.55 \\ d(i), & d(i) \geq 0.55 \end{cases}, \quad d(i) = \max_{0 \leq j \leq 2} \left| f^j_{shape}(i+1) + f^j_{shape}(i-1) - 2 f^j_{shape}(i) \right|$$

in which  $f_{shape}^{j}(i)$  is the value of  $f_{shape}$  of the ith element in the jth parametric direction. The definition of  $f_{shape}$  [39] can be referred to Appendix.2 for details.

**Width term.** The width term  $E_{sd}$  in the weighted ranking function measures the width of sheet. If the sheet is too wide, the collapsing operation will lead to big distortion on the boundary geometry and affect the adjacent sheets seriously. Hence it is reasonable to remove sheets with thin shape. For this term, we use the width of base-complex edges in  $E_M$ , which is more accurate than the length between the vertex pair on surface. Based on the observation, some base-complex sheets with locally thin shape will be difficult to identify in the original method. In our framework,  $E_{sd}$  is defined by combining the average width and the minimum length, and the cube root form is used to reduce the effect of actual values.  $E_{sd}$  is defined as

$$E_{sd} = \left[ \left( \alpha_a \min_{(v_l, v_r) \in P_V} d(v_l, v_r) + \alpha_b \bar{d} \right) / \bar{L} \right]^{1/3}$$
(12)

in which  $\bar{L}$  is the average length of the base-complex edges,  $d(v_{\bar{l}}, v_r)$  is the length of the base-complex edge connecting  $v_l$  and  $v_r$ ,  $\bar{d}$  is the average length of the base-complex edges in  $E_M$  of this base-complex sheet, and we choose  $\alpha_a=0.7$  and  $\alpha_b=0.3$  in our experiments.

## 5.2. Ranking approach for base-complex chord

The base-complex chord collapsing operation only influences one column of components, which is used to adjust regions with many edge pairs having a valence of  $3\sim5$ . From our observation, edge pair with a valence of  $3\sim5$  often exists in the entangled

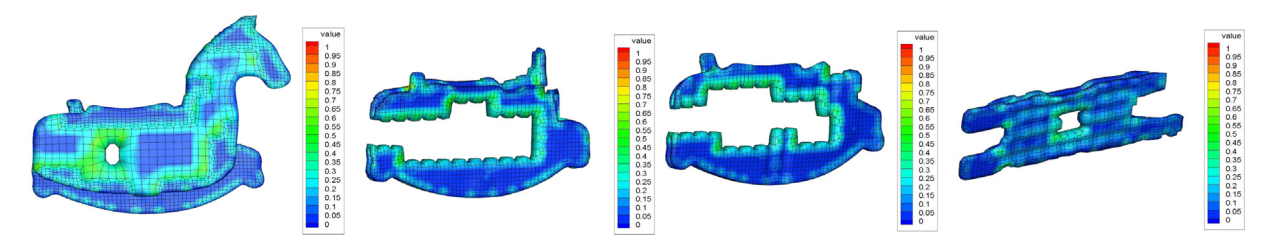


**Fig. 6.** Color mapping of the second derivative of  $f_{shape}$  for four base-complex sheets. The second derivative of  $f_{shape}$  is larger than 0.55 for regions with more serious twist

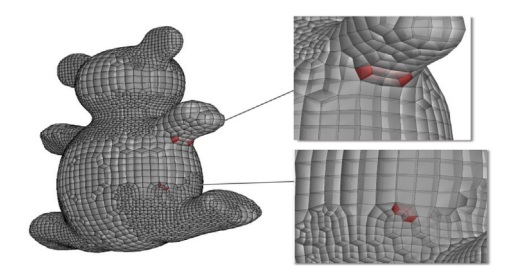


**Fig. 7.** Two base-complex chords (red) in a toy mesh. The first chord is located in a patch near the feature edges (top right), and the second chord is located in the flat region (bottom right). The elimination of the first chord will lead to a significant boundary geometry error. The proposed geometric error term can prevent this kind of collapsing operation effectively.

sheets, which is difficult to eliminate. In order to untangle them, we propose a priority metric  $E_c(c)$ .  $E_c(c)$  does not contain the distortion term, because the elimination of base-complex chords only has impact on local regions. The formula of  $E_c(c)$  is defined as

$$E_c(c) = k_{cq}(1 - e^{-E_{cq}(c)}) + k_{cv}(1 - e^{-E_{cv}(c)})$$
(13)

in which  $E_{cv}$  is the valence term and  $E_{cq}$  is the geometry error term,  $k_{cq}$  and  $k_{cv}$  are set to be 0.6 and 0.4 respectively in our experiments.

**Geometry error term.** The chord collapsing operation often leads to simplification results with inverted elements. We propose a simple strategy for priority processing on chords with narrow shape and smaller length. The aspect ratio of a chord is defined as the ratio of the average length of the main diagonal to the sub-diagonal, which is applied to the measurement of thickness. To reduce the collapsing effect on boundary geometry, Gaussian curvature [40] is used to measure the shape error locally after collapsing. In our implementation, we use the variance of curvature to find patches with significant curvature changes. A patch may contain sharp features when its variance of curvature is large as shown in Fig. 7. The geometry error term  $E_{cq}(c)$  is defined as

$$E_{cq}(c) = \frac{L_1(c)}{\bar{l}L_2(c)} \sqrt{\frac{\sum_{i=1}^{N_v} (Q_{gi} - \bar{Q_g})^2}{N_v - 1}}$$
(14)

in which  $L_1, L_2$  are the average length of the main diagonal and the sub-diagonal respectively,  $\bar{l}$  is the average length of elements,  $Q_{gi}$  is the Gaussian curvature of a vertex on two sides (two sides of the chord are the set of faces in the boundary, and their normals are parallel to the direction of the dual string.) and  $\bar{Q_g}$  is the average Gaussian curvature of vertices on two sides.

**Valence error term**. The valence error term measures the valence error of four topological parallel edges, and uses the same form as the valence term for base-complex sheet. To eliminate entangled sheets and simplify the local complexity, three topological parallel edges created by collapsing should be all regular.

The ideal situation is that the valence error tends to be zero. In our framework, the valence error is set as one of the optimization objectives, and the valance error of base-complex chord in the collapsing operation is provided in Section 4 as D(c), and  $1/N_b(c)$  can be used as the normalization coefficient naturally. The valence error term  $E_{cv}$  is defined as

$$E_{cv}(c) = D(c)/3N_b(c), \tag{15}$$

in which  $N_b(c)$  is the number of base-complex components in base-complex chord c.

#### 6. Sheet refinement

Sheet refinement is performed during the simplification pipeline in order to maintain the input mesh geometry with the user-defined target number of elements. A similar method in [9] can be used to split one element on a specific sheet into two elements along the direction perpendicular to the parallel edges. In this paper, we propose an adaptive sheet refinement method to improve the accuracy of boundary geometry approximation.

In our implementation, we find that choosing a sheet with the maximum width to refine is not a robust strategy, where some boundary patches with large boundary approximation error may not be refined. In our method, we firstly obtain the average length of all edges along the collapsing direction, and then compute the average Hausdorff distance ratio HR(s) by the means of point sampling for each sheet in the priority queue. According to the descending order of HR(s), the first four basecomplex sheets will be selected in advance, and the average length in the collapsing direction is denoted as  $L_b$ . We choose one from the first four sheets to perform refinement if  $L_b > 1.2L$ ; otherwise, we refine the candidate with the maximum  $\bar{L_b}$  and meeting the above condition. During simplification, collapsing operations may fail frequently due to the element quality and shape error constrains. In order to relax these constrains, we also perform the refinement process when a sheet collapsing fails. The base-complex sheets sharing  $F_L$  and  $F_R$  with the removed sheet are selected as candidates. The refinement process narrows the parameterized region of failed sheets, such that it reduces the shape error by introducing more elements, and the sheet may be collapsed in the next iteration. In addition, another criterion is introduced to control the number of elements strictly. For the input hex-mesh with  $C_0$  elements, if the target number is  $C_n$ before performing refinement, we check whether the number of hexahedra contained in a sheet is less than  $1.5 \times (C_0 - C_n)$ . This criterion can effectively prevent some sheets being refined repeatedly.

## 7. Experimental results

The proposed algorithm has been tested on a four-core i7 processor with 8 GB memory. The maximal number of iterations of the SLIM solver is set as 5, and HR = 1% (the threshold of the Hausdorff distance ratio defined by the user, the simplification

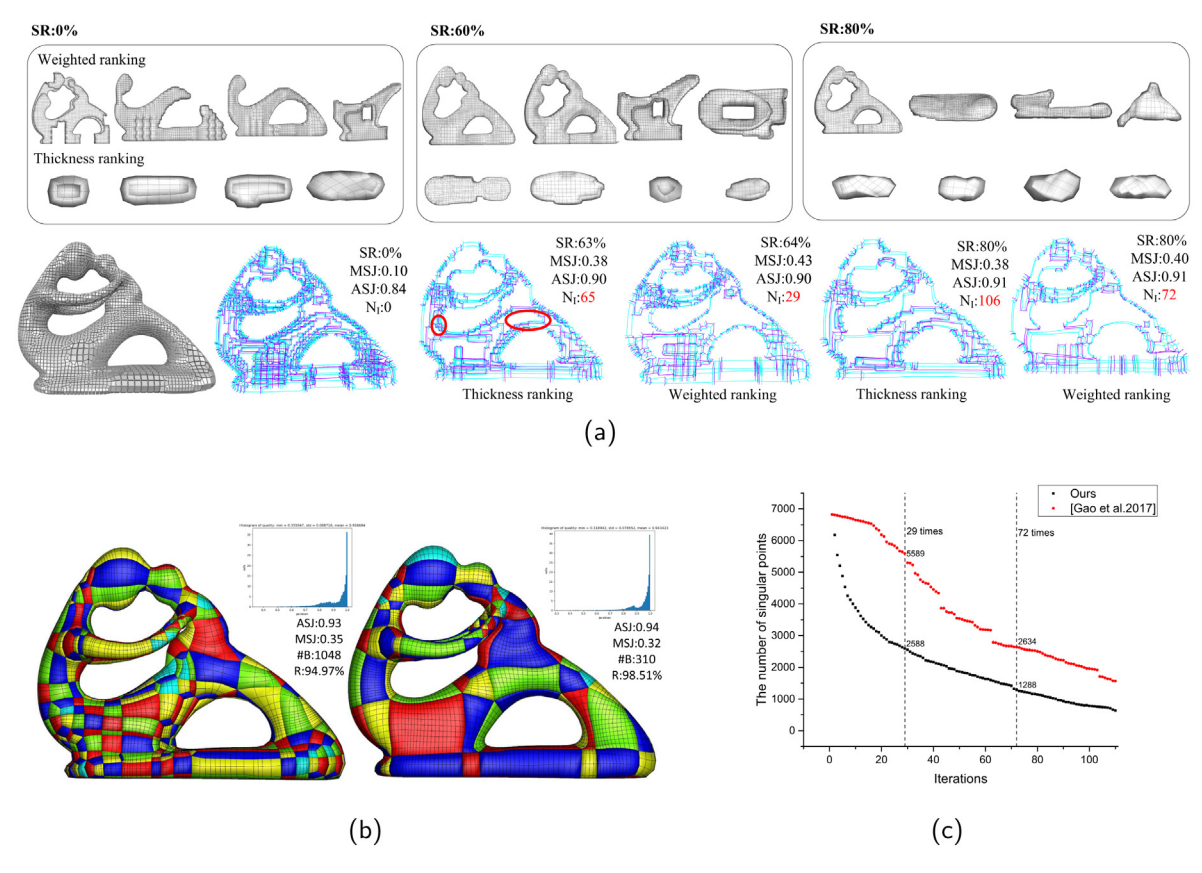


**Fig. 8.** Simplification results of the fertility mesh with different complexity reductions, including our weighted ranking approach and the thickness ranking method [9] as shown in (a). Our ranking method can effectively decrease the iteration steps ( $N_1$ ) and improve the simplification results around regions with dense singularities as shown in the singular structure highlighted with red circles. The top 4 candidates in each sequence are also shown when the simplification rates (SR) achieve 0%, 60% and 80%. The simplification results are shown in (b), and the statistics of iterations are shown in (c). (For interpretation of the references to color in this figure legend, the reader is referred to the web version of this article.)

rate becomes larger when HR increases) and  $r_{|H|}=1.0$  (the rate of the target number over the number of hex-elements in the input mesh) for all experiments. We also report the number of hex elements (#H), the number of base-complex components (#BC) and the minimal, average and standard variance value of scaled Jacobians (MSJ/ASJ/Std). The boundary geometry error is measured by the Hausdorff distance ratio (HR). We have tested the proposed method on 165 hex-mesh models, the average simplification rate for these meshes is 88%, which is higher than the approaches in [8] and [9].

Weighted ranking candidates. Simplification results of the thickness ranking method [9] and the proposed weighted ranking method will be compared. In Fig. 8(a), we show top 4 candidates in the fertility mesh when the simplification rates achieve 0%, 60% and 80% respectively. In the initial priority queue, our weighted ranking term can effectively pick up base-complex sheets with serious distortion and close-loop configurations. Moreover, the number of singularities can also be reduced faster. For a simplification rate of 60%, the thickness ranking method needs 65 iterations, and our proposed method only needs 28 iterations. For the comparison results as shown in Fig. 8(a), when the simplification rates reach 60% and 80%, our ranking algorithm can preferentially remove sheets to promote singular edge elimination, and the regions with dense singularities (marked with red circles) have been greatly improved. Compared with the simplification results by the thickness ranking, regions with dense singular edges can be successfully eliminated by our method, and self-intersected sheets can be removed as well at the same time. In the simplification process, the distortion term is used to eliminate elements with poor shape quality, and to spread the distortion to neighboring elements while gradually improving the value of MSJ/ASJ in the hex-mesh. ASJ with the proposed method is better than thickness ranking during these three stages, 12.66% ASJ improvement over the input and 2.20% ASJ improvements over the simplification result by [9] can be achieved. The average running time of the entire dataset is 71 minutes, which is slightly slower than [9].

There are quite few candidates in the simplification queue when the reduction ratio reaches 90%, and the number of candidates is also limited by geometrical constrains, which will cause more incorrect collapsing and need more time consumption. The pipeline of [9] uses a simple strategy by skipping a set number of candidates to improve the speed, but it may cause early termination.

**Ranking terms**. In this paper, several ranking terms for collapsing base-complex sheets have been proposed. In Fig. 9, simplification results by two terms for base-complex sheets are compared. As shown in the second row of Fig. 9, the proposed valence term has some advantages to improve the simplification ratio in fewer iterative steps, However, if we only use the valence term, more failed collapsing operations will be introduced to reach the threshold of the Hausdorff distance ratio, and it also leads to a simplified mesh with a lower value of MSJ. The result by using the valence term is shown in the last column in Fig. 9. The width term plays an assistance role for the valence term to avoid serious shape error, the proposed new width term can lead to a more uniform distribution of elements when it is compared with [9] as shown in the third column of Fig. 9. The MSJ value is improved significantly compared with the result of [9], and the original width ranking approach may result in an unexpected

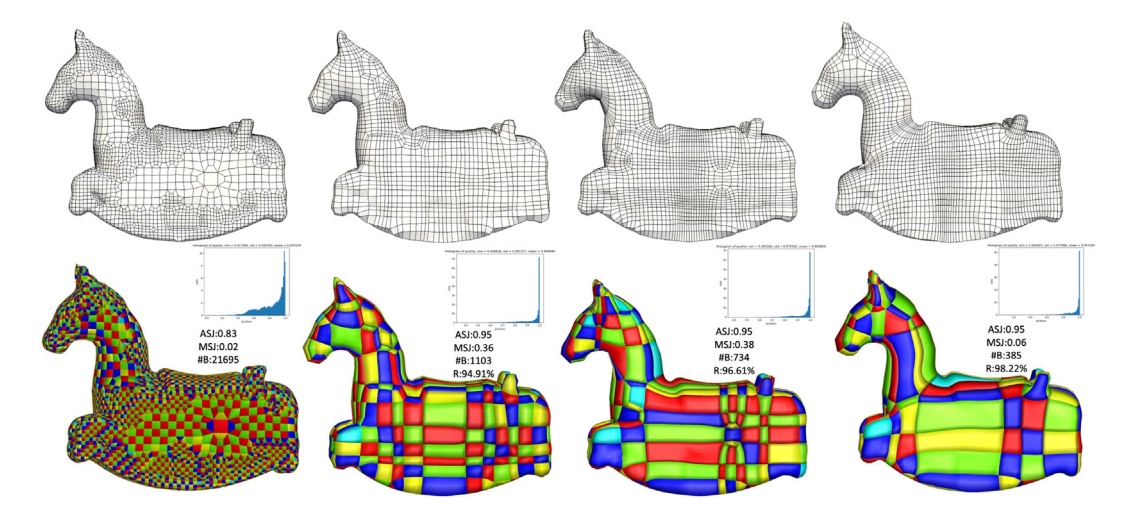


Fig. 9. Simplification results on an isidore horse hex-mesh generated by the octree-based method. The hex-mesh and base-complex structure of input, result of the method in [9], result of the method based on the new width term and result of the approach based on the valence term are shown from left to right respectively.

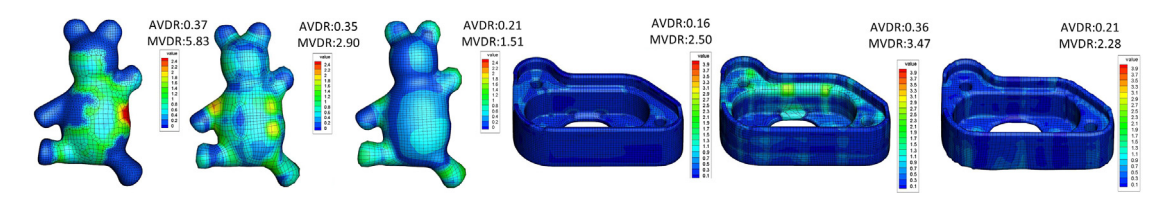
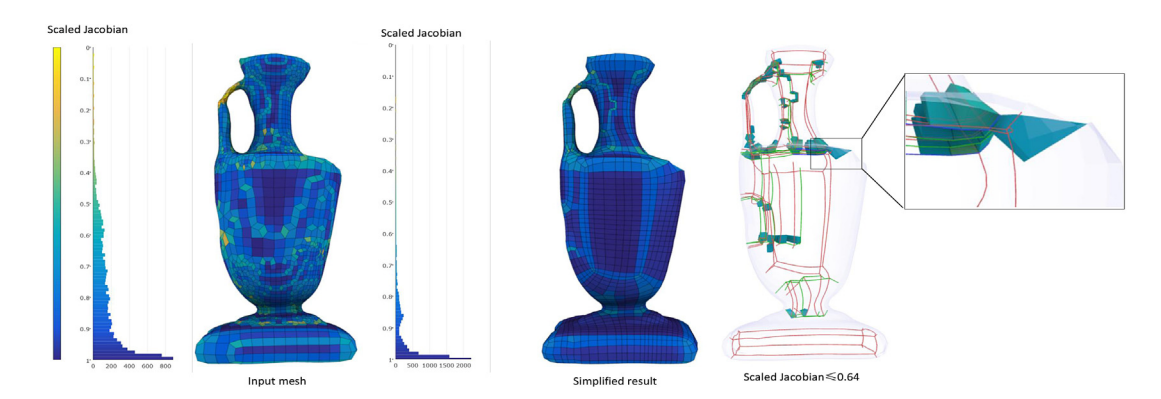


Fig. 10. Simplification results of toy and lock. From left to right, the input meshes, results of thickness ranking [9] and our weighted ranking results are shown respectively. The color mapping shows the value of VDR, which illustrates that our weighted ranking method can achieve a significant improvement on uniformity.



**Fig. 11.** Simplification result on bottle mesh generated by the octree-based method. The scaled Jacobian of the input mesh, the simplified result and elements with scaled Jacobian less than 0.64 are shown from left to right, respectively. As shown in the enlarged region, there are a few poorly shaped elements which are mainly around singular edges with high valence.

exception since the thick sheet with narrow localized regions cannot be removed.

**Element uniformity.** In the proposed approach, local parameterization is used to improve the uniformity of hex-mesh elements. We also propose a measurement of element uniformity called the *volume deviation ratio* (VDR), which is defined as the standard volume deviation of neighboring elements divided by the average element volume. The range of VDR is  $(0, \infty]$ , and the uniformity is better while the value is closer to 0 (for all elements with the same volume, VDR=0). Compared with the thickness ranking method [9], our simplification results have 30.17% and 7.04% improvement in the average volume deviation ratio (AVDR) and the max volume deviation ratio (MVDR). In our experiments, the average AVDR and MVDR of meshes from polycube-base methods are 0.19 and 2.78 respectively, and the average AVDR/MVDR are 0.25/2.54 in the simplification results

of octree-base meshes. AVDR and MVDR gain 35.56% and 10.86% improvement compared with the thickness ranking approach for octree-based meshes. Two comparison examples are shown in Fig. 10 with the VDR colormap.

In the proposed framework, hex-elements with low quality mainly distribute near the edges with high valence, which can be promoted by the optimization approach introduced in [34] and [43]. In Fig. 11, the Jacobian quality colormap of a bottle mesh is shown, and we can observe that elements with Jacobian lower than 0.64 are neighboring to the edges with high valence.

**Simplification of hex-meshes generated by polycube-based methods.** For hex-meshes generated by polycube-based methods [21,26,41], the singularity structures are completely distributed on the boundary surface, and the distribution of singular edges is sparse. Hence, the valence term has a small contribution, and the weights  $k_{sd}$  and  $k_{sv}$  are set as  $k_{sd} = 0.6$  and  $k_{sv} = 0.4$ 



**Fig. 12.** Simplification results on meshes generated by the polycube-based method, the gargoyle mesh (left) is generated by [41], and the casting mesh (right) is generated by [42]. From top to bottom, the input hex-mesh, simplification results of thickness ranking [9] and our weighted ranking results are presented. For each example, we show the information of scaled Jacobian, singularity structure, and the base-complex components with different colors.

**Table 1**Statistics of meshes generated by octree-based methods.

Model	Input hex mesh					Simplified result							
	#H	#BC	MSJ	ASJ	Std	#H	#BC	MSJ	ASJ	Std	HR (%)	R (%)	Time (m)
Bimba (Fig. 13)	25,347	25,347	0.06	0.80	0.162	23,840	171	0.43	0.97	0.051	0.96	99.33	69.50
Bottle (Fig. 13)	35,886	35,860	0.13	0.79	0.167	34,484	121	0.37	0.98	0.046	0.93	99.66	104.01
Deckle (Fig. 13)	53,658	53,116	0.03	0.84	0.187	48,674	902	0.48	0.96	0.072	0.99	98.30	452.90
Fertility (Fig. 8)	21,370	20,840	0.10	0.84	0.150	21,016	310	0.32	0.94	0.079	0.87	98.51	153.83
Toy1 (Fig. 7)	18 947	18 883	0.12	0.81	0.161	18 656	323	0.45	0.96	0.059	0.95	98.29	38.20
Toy2 (Fig. 10)	14,288	14,288	0.15	0.81	0.158	13,476	173	0.43	0.96	0.058	0.92	98.79	30.79
Lock (Fig. 10)	28,753	25,720	0.01	0.80	0.244	26,555	2058	0.33	0.94	0.109	0.97	92.00	369.07

in our experiments. As shown in Fig. 12 and Table 2, the proposed approach can achieve a higher base-complex component reduction with similar element quality as the results in [9]. In our experiments, the average scaled Jacobian is improved to 0.96, and the meshes obtain 30.17%/7.04% improvement for AVDR and MVDR compared with the thickness ranking approach [9]. Moreover, the average component reduction ratio is promoted to 63.81%, and some results are very similar with the structure of meshes generated by [33].

Simplification of hex-meshes from octree-based methods. Octree-based hex-meshing approaches often generate a complex structure with dense local singularities. In [9], the greedy collapsing by thickness ranking was utilized under a set of filters. It cannot find a coarser structure in the hex-mesh with a large number of interior singularities, since the thickness ranking term does not have a direct effect on singularity removal. The corresponding simplification [9] has a slow convergence rate, and it can achieve an average simplification rate around 86% for the hex-mesh database. The proposed weighted ranking method can

obtain a much simpler singularity structure with much fewer base-complex components. The average simplification rate in the proposed framework can increase 89.24% with respect to the initial number of base-complex components in the input hexmesh, and gain 3.24% improvement compared with [9]. Moreover, in the proposed framework, adaptive refinement is performed during the simplification process, which can effectively maintain the quality of boundary geometry and promote the simplification process under the constraint of *HR*. Our ASJ/MSJ achieves 0.91/0.28, and gain 11.57% ASJ improvements over the thickness ranking method. Some simplification results are shown in Fig. 13, and statistics are presented in Table 1. Comparison examples with [9] are also presented in Fig. 14 and Table 2.

#### 8. Conclusion and future work

In this paper, an improved singularity structure simplification method is proposed for hex-meshes based on a weighted ranking function, which is a combination of the valence prediction

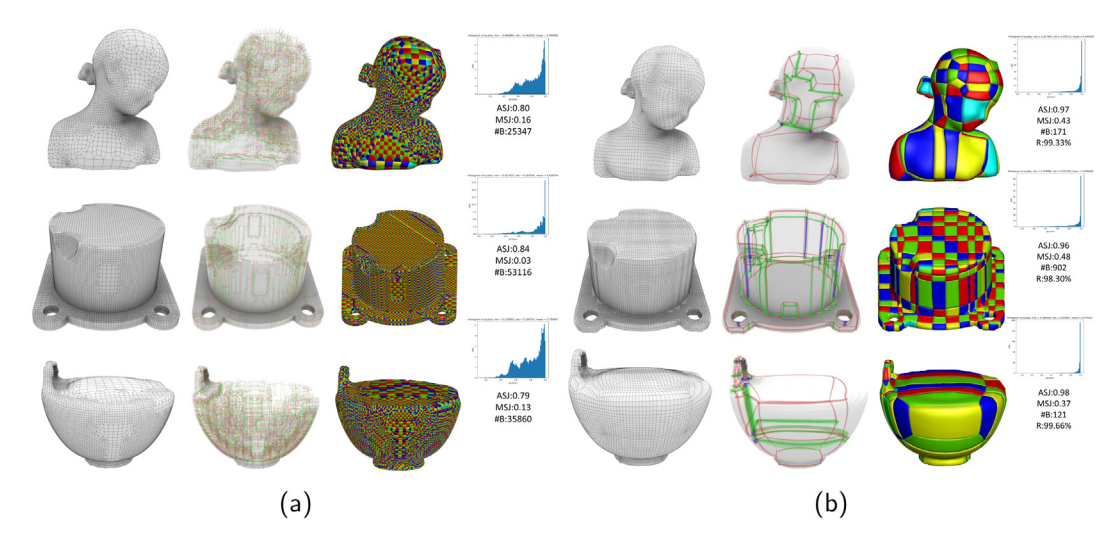


**Fig. 13.** Simplification results on meshes generated by octree-based methods, including the bimbia, deckel and bottle models. From left to right, the input mesh, singularity structure (the singular edges with a valence of 5 marked in green, and a valence of 3 marked in red, the valence of edges with other colors is greater than 5), base-complex of original meshes (a) and simplified results (b). (For interpretation of the references to color in this figure legend, the reader is referred to the web version of this article.)

**Table 2**Comparison with [9]. #H is the number of hex-elements, #BC is the number of base-complex components, Std is the standard deviation of the scaled Jacobians, HR stands for the Hausdorff distance, and R is the simplification rate.

Model		#H	#BC	MSJ	ASJ	Std	AVDR	MVDR	HR (%)	R (%)	Time (m)
	Input	25,669	7,563	0.20	0.91	0.907	0.11	0.64			
Gargoyle (Fig. 12)	Thickness ranking	22,524	805	0.14	0.96	0.068	0.30	3.52	0.98	89.36	30.67
	Weighted ranking	25,034	451	0.33	0.96	0.068	0.19	1.79	0.91	92.75	51.52
Casting (Fig. 12)	Input	21,167	2,805	0.20	0.85	0.016	0.05	1.29			
	Thickness ranking	15,123	1,562	0.11	0.92	0.012	0.10	2.74	0.83	44.31	7.53
	Weighted ranking	18,522	595	0.34	0.93	0.082	0.26	1.74	0.94	78.79	30.68
Rocker (Fig. 14)	Input	16,608	16,487	0.11	0.86	0.139	0.18	2.69			
	Thickness ranking	10,278	636	0.44	0.93	0.081	0.38	1.77	0.99	96.14	32.25
	Weighted ranking	14,996	367	0.55	0.95	0.070	0.24	2.25	0.88	97.77	52.42
Pig (Fig. 14)	Input	13,987	13,987	0.02	0.79	0.168	0.46	8.02			
	Thickness ranking	10,704	2,305	0.23	0.92	0.102	0.38	3.89	0.99	83.52	31.24
	Weighted ranking	11,144	880	0.39	0.94	0.082	0.24	1.49	0.98	93.71	33.01
Bird (Fig. 14)	Input	4,247	3,640	0.03	0.82	0.159	0.18	0.51			
	Thickness ranking	2,868	580	0.24	0.90	0.117	0.36	2.43	1.00	84.07	14.57
	Weighted ranking	4,336	312	0.34	0.92	0.102	0.21	1.23	0.92	91.43	10.85
Buste (Fig. 14)	Input	19,075	18,355	0.13	0.85	0.151	0.28	3.20			
	Thickness ranking	17,680	691	0.44	0.95	0.070	0.33	4.36	0.98	96.24	113.67
	Weighted ranking	17,324	221	0.53	0.97	0.055	0.22	1.62	0.90	98.80	38.31

function of local singularity structure, shape quality metric of elements and the width of base-complex sheets/chords. Local optimization and adaptive sheet refinement are also proposed to improve the element quality of simplified hex-mesh. Compared with the thickness ranking method, simpler singularity structure with fewer base-complex components can be achieved while achieving better mesh quality and Hausdorff distance ratio. The proposed approach has a few limitations, for examples, sharp features cannot be preserved very well on the boundary, and the boundary approximation could be improved for models with high genus. In the future, we can also apply the proposed hexmesh simplification method to volume parameterization problems [44–46], which is a bottleneck in isogeometric analysis.

## **Declaration of competing interest**

The authors declare that they have no known competing financial interests or personal relationships that could have appeared to influence the work reported in this paper.

#### Acknowledgments

The authors thank the anonymous reviewers for providing constructive suggestions and comments, that contributed to highly improve this work. The authors appreciate the joint support for this project by the National Natural Science Foundation of China (Grant Nos. 61761136010, 61772163, 61802099), the Science Challenge Project, China (Grant No. TZ2016002), the NSFC-Zhejiang Joint Fund for the Integration of Industrialization and Informatization, China (Grant No. U1909210), and the Zhejiang Lab Tianshu Open Source AI Platform.

## Appendix A

Energy minimizing equation

The three terms  $E_D(V)$ ,  $E_T(V)$  and  $E_B(V)$  in E(V) are denoted as follows:

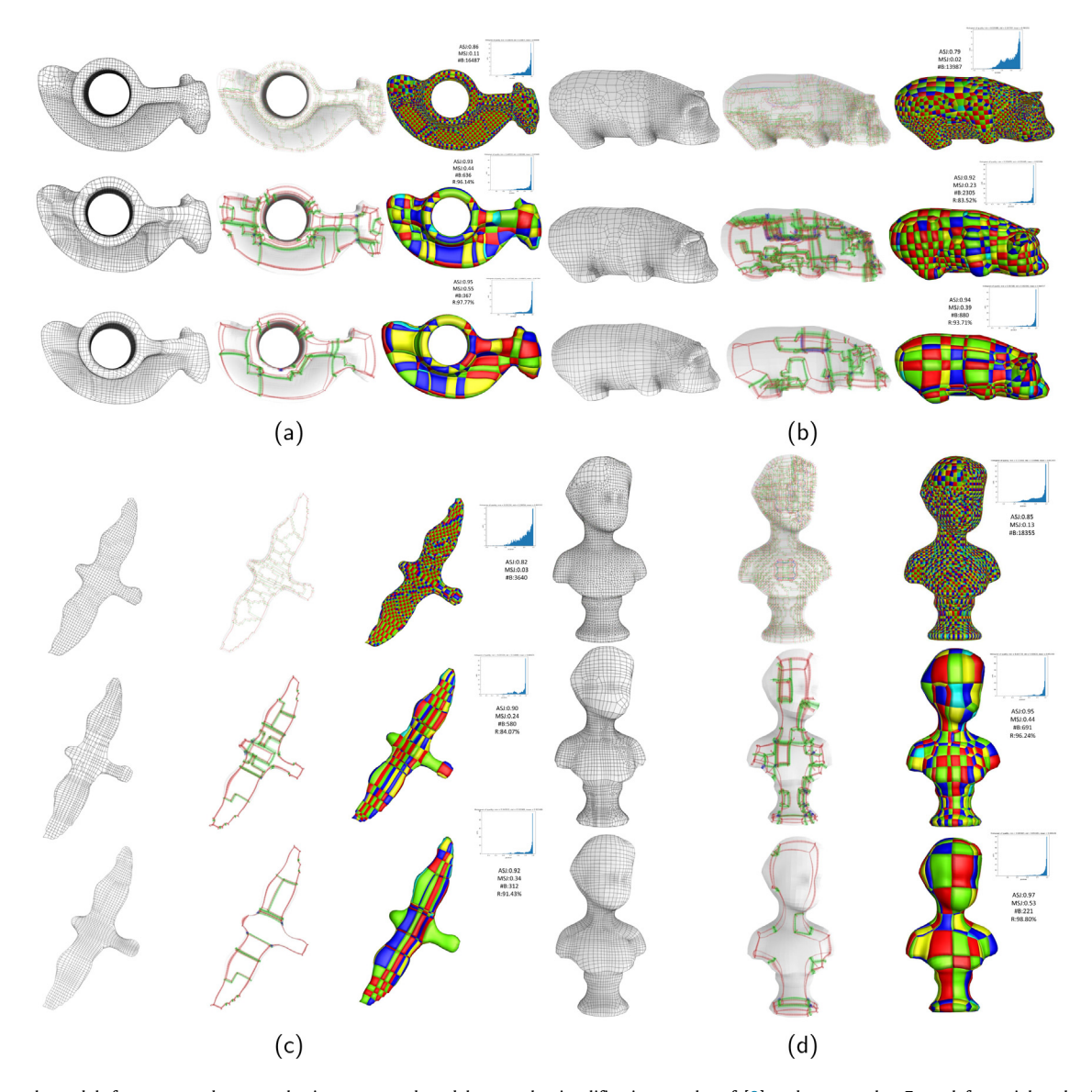


Fig. 14. For each model, from top to bottom: the input octree-based hex-mesh, simplification results of [9] and our results. From left to right: the input mesh, singularity structure, and base-complex. We show the scaled Jacobian, singularity structure, and base-complex components with different colors.

$$E_D(V) = \sum_{h \in H} \sum_{t \in h} M_t(\|J_t\|_F^2 + \|J_t^{-1}\|_F^2),$$

where H is the parameterization region, h is an element in H, and t is one of the eight tetrahedra in h (each tetrahedron is related with a corner of h),  $J_t$  is the Jacobian of the transformation from the original shape to the ideal shape of t.

$$E_t(V) = \sum_{i=1}^K \sum_{i=1}^{K_i} \|v_{i,j} - \bar{v}_i\|^2,$$

where K is the number of groups of collapsing vertices,  $K_i$  is the number of vertices in a group,  $v_{i,j}$  is the jth vertex in the ith group, the vertices in the ith group will be collapsed to the new position  $\bar{v}_i$ , and  $\bar{v}_i$  is located in the dual surface sheet.

$$E_B(V) = \sum_{v \in C} \|v - \bar{v}\|^2 + \sum_{v \in L} \|v - \bar{v} - a_l \vec{d}_l\|^2 + \sum_{v \in S} \|\vec{n}(v - \vec{v})\|^2,$$

where C, L, and S are the set of corner vertices, feature line vertices, and regular vertices respectively, vertex v is located on

the boundary, and  $\bar{v}$  is the closet surface position for v,  $\vec{d}_l$  is the feature line tangent at  $\bar{v}$ ,  $\vec{n}$  is the normal of  $\bar{v}$ .

Shape metric

A hexahedral element has eight nodes, the kth node can form a Jacobian matrix  $A_k$ ,  $k=0,1,\ldots,7$ , and  $\alpha_k=det(A_k)$  is the local tetrahedron volume associated with the kth node.  $A_k$  has the following form:

$$A_k = (-1)^k \begin{bmatrix} x_{k+1} - x_k & x_{k+2} - x_k & x_{k+3} - x_k \\ y_{k+1} - y_k & y_{k+2} - y_k & y_{k+3} - y_k \\ z_{k+1} - z_k & z_{k+2} - z_k & z_{k+3} - z_k \end{bmatrix},$$

in which  $x_{k+i}$ ,  $y_{k+i}$ ,  $z_{k+i}$ , i=1,2,3 are the coordinates of the kth node's three neighboring nodes. We can construct a metric tensor  $A_k^T A_k$  in the form of  $3 \times 3$  symmetric matrix, and each matrix contains six different elements. The  $\lambda_{ij}^k$ , i,j=1,2,3, is the ijth element of the kth metric tensor. The shape quality metric for a hexahedron with a cubical reference element is

$$f_{shape} = \frac{24}{\sum_{k=0}^{7} (\lambda_{11}^{k} + \lambda_{22}^{k} + \lambda_{33}^{k})/(\alpha_{k}^{2/3})}$$

This metric depends on both element angle and length ratio, and can measure the shape distortion of a hexahedron.  $f_{shape}$  has the property of scale-invariance, the hexahedron is a cube when  $f_{shape} = 1$ , and the hexahedron is degenerated when  $f_{shape} = 0$ .

#### References

- [1] Wei X, Zhang YJ, Hughes TJR. Truncated hierarchical tricubic c0 spline construction on unstructured hexahedral meshes for isogeometric analysis applications. Comput Math Appl 2017;74(9):2203–20, A Special Issue of Advances in Mathematics of Finite Elements in Honor of Ivo Babuska in.
- [2] Wei X, Zhang YJ, Toshniwal D, Speleers H, Li X, Manni C, et al. Blended b-spline construction on unstructured quadrilateral and hexahedral meshes with optimal convergence rates in isogeometric analysis. Comput Methods Appl Mech Engrg 2018;341(1):609–39.
- [3] Zhang Y, Bajaj C. Adaptive and quality quadrilateral/hexahedral meshing from volumetric data. Comput Methods Appl Mech Engrg 2006;195(9– 12):942–60.
- [4] Ito Y, Shih AM, Soni BK. Octree-based reasonable-quality hexahedral mesh generation using a new set of refinement templates. Internat J Numer Methods Engrg 2010;77(13):1809–33.
- [5] Qian J, Zhang Y. Automatic unstructured all-hexahedral mesh generation from b-reps for non-manifold cad assemblies. Eng Comput 2012;28(4):345–59.
- [6] Bourdin X, Trosseille X, Petit P, Beillas P. Comparison of tetrahedral and hexahedral meshes for organ finite element modeling: an application to kidney impact. In: 20th international technical conference on the enhanced safety of vehicle. 2007.
- [7] Woodbury AC, Shepherd JF, Staten ML, Benzley SE. Localized coarsening of conforming all-hexahedral meshes. Eng Comput 2011;27(1):95–104.
- [8] Gao X, Deng Z, Chen G. Hexahedral mesh re-parameterization from aligned base-complex. ACM Trans Graph 2015;34(4):142.
- [9] Gao X, Panozzo D, Wang W, Deng Z, Chen G. Robust structure simplification for hex re-meshing. ACM Trans Graph 2017;36(6):185.
- [10] Rabinovich M, Poranne R, Panozzo D, Sorkine-Hornung O. Scalable locally injective mappings. ACM Trans Graph 2017;36(2):16.
- [11] Shepherd JF. Topologic and geometric constraint-based hexahedral mesh generation, Vol. 68 (PhD Dissertation), University of Utah; 2007.
- [12] Roca Navarro X. Paving the path towards automatic hexahedral mesh generation (PhD Dissertation), Universitat Politècnica de Catalunya; 2009.
- [13] Wu H, Gao S, Wang R, Chen J. Fuzzy clustering based pseudo-swept volume decomposition for hexahedral meshing. Comput Aided Des 2018;96: 42–58.
- [14] Zhang Y, Bazilevs Y, Goswami S, Bajaj CL, Hughes TJ. Patient-specific vascular NURBS modeling for isogeometric analysis of blood flow. Comput Methods Appl Mech Engrg 2007;196(29–30):2943–59.
- [15] Blacker TD, Meyers RJ. Seams and wedges in plastering a 3D hexahedral mesh generation algorithm. Eng Comput 1993;9(2):83–93.
- [16] Owen SJ, Saigal S. H-morph: an indirect approach to advancing front hex meshing. Internat J Numer Methods Engrg 2015;49(1-2):289–312.
- [17] Tautges TJ, Blacker T, Mitchell SA. The whisker weaving algorithm: a connectivity-based method for constructing all-hexahedral finite element meshes. Internat J Numer Methods Engrg 1996;39(19):3327–49.
- [18] Ledoux F, Weill J-C. An extension of the reliable whisker weaving algorithm. In: Proceedings of the 16th international meshing roundtable. Springer; 2008, p. 215–32.
- [19] Staten ML, Kerr RA, Owen SJ, Blacker TD, Stupazzini M, Shimada K. Unconstrained plastering hexahedral mesh generation via advancingfront geometry decomposition. Internat J Numer Methods Engrg 2010;81(2):135–71.
- [20] Schneiders R. An algorithm for the generation of hexahedral element meshes based on an octree technique. In: 6th international meshing roundtable. 1997, p. 195–6.
- [21] Gregson J, Sheffer A, Zhang E. All-hex mesh generation via volumetric polycube deformation. Comput Graph Forum 2011;30(5):1407–16.

- [22] Liu L, Zhang Y, Liu Y, Wang W. Feature-preserving T-mesh construction using skeleton-based polycubes. Comput Aided Des 2015;58:162–72.
- [23] Fu X, Bai C, Liu Y. Efficient volumetric polycube-map construction. Comput Graph Forum 2016;35(7):97–106.
- [24] Hu K, Zhang YJ. Centroidal Voronoi tessellation based polycube construction for adaptive all-hexahedral mesh generation. Comput Methods Appl Mech Engrg 2016;305:405–21.
- [25] Hu K, Zhang YJ, Liao T. Surface segmentation for polycube construction based on generalized centroidal Voronoi tessellation. Comput Methods Appl Mech Engrg 2017;316:280–96.
- [26] Fang X, Xu W, Bao H, Huang J. All-hex meshing using closed-form induced polycube. ACM Trans Graph 2016;35(4):124.
- [27] Nieser M, Reitebuch U, Polthier K. Cubecover-parameterization of 3D volumes. Comput Graph Forum 2011;30(5):1397–406.
- [28] Huang J, Tong Y, Wei H, Bao H. Boundary aligned smooth 3D cross-frame field. ACM Trans Graph 2011;30(6):1–8.
- [29] Li Y, Liu Y, Xu W, Wang W, Guo B. All-hex meshing using singularity-restricted field. ACM Trans Graph 2012;31(6):1–11.
- [30] Wu Y, He Y, Cai H. QEM-based mesh simplification with global geometry features preserved. In: International conference on computer graphics and interactive techniques in australasia and southeast asia. 2004, p. 50–7.
- [31] Tarini M, Pietroni N, Cignoni P, Panozzo D, Puppo E. Practical quad mesh simplification. Comput Graph Forum 2010;29(2):407–18.
- [32] Shepherd JF, Dewey MW, Woodbury AC, Benzley SE, Staten ML, Owen SJ. Adaptive mesh coarsening for quadrilateral and hexahedral meshes. Finite Elem Anal Des 2010;46(1–2):17–32.
- [33] Cherchi G, Livesu M, Scateni R. Polycube simplification for coarse layouts of surfaces and volumes. Comput Graph Forum 2016;35(5):11–20.
- [34] Wang R, Gao S, Zheng Z, Chen J. Hex mesh topological improvement based on frame field and sheet adjustment. Comput Aided Des 2018;103:103–17.
- [35] Daniels J, Silva CT, Cohen E. Semi-regular quadrilateral-only remeshing from simplified base domains. In: Computer graphics forum, Vol. 28. Wiley Online Library; 2009, p. 1427–35.
- [36] Liu L, Zhang L, Xu Y, Craig G, Steven GJ. A local/global approach to mesh parameterization. In: Computer graphics forum, Vol. 27. Wiley Online Library; 2008, p. 1495–504.
- [37] Liao SH, Tong RF, Dong JX, Zhu FD. Gradient field based inhomogeneous volumetric mesh deformation for maxillofacial surgery simulation. Comput Graph 2009;33(3):424–32.
- [38] Daniels J, Silva CT, Shepherd J, Cohen E. Quadrilateral mesh simplification. ACM Trans Graph 2008;27(5):148.
- [39] Knupp PM. Algebraic mesh quality metrics for unstructured initial meshes. Finite Elem Anal Des 2003;39(3):217–41.
- [40] Xu G. Convergence analysis of a discretization scheme for Gaussian curvature over triangular surfaces. Comput Aided Geom Design 2006;23(2):193–207.
- [41] Huang J, Jiang T, Shi Z, Tong Y, Bao H, Desbrun M. L1-based construction of polycube maps from complex shapes. ACM Trans Graph 2014;33(3):1-11.
- [42] Livesu M, Vining N, Sheffer A, Gregson J, Scateni R. Polycut: monotone graph-cuts for polycube base-complex construction. ACM Trans Graph 2013:32(6):1–12.
- [43] Livesu M, Sheffer A, Vining N, Tarini M. Practical hex-mesh optimization via edge-cone rectification. ACM Trans Graph 2015;34(4):141.
- [44] Xu G, Li M, Mourrain B, Rabczuk T, Xu J, Bordas SPA. Constructing IGAsuitable planar parameterization from complex CAD boundary by domain partition and global/local optimization. Comput Methods Appl Mech Engrg 2018;328:175–200.
- [45] Xu G, Kwok TH, Wang CCL. Isogeometric computation reuse method for complex objects with topology-consistent volumetric parameterization. Comput Aided Des 2017;91:1–13.
- [46] Xie J, Xu JL, Dong ZY, Xu G, Deng CY, Mourrain B, et al. Interpolatory Catmull-Clark volumetric subdivision over unstructured hexahedral meshes for modeling and simulation applications. Comput Aided Geom Design 2020;80:101867.